Rapid antibiotic susceptibility determination by fluorescence lifetime tracking of bacterial metabolism

Journal:	*ACS Infectious Diseases*
Manuscript ID	id-2024-00491j.R2
Manuscript Type:	Letter
Date Submitted by the Author:	n/a
Complete List of Authors:	Rojas-Andrade, Mauricio; University of California Irvine, Materials Science and Engineering Perinbam, Kumar; University of California Irvine Nguyen, Quan Thanh; University of California Irvine Kim, Jonathan; University of California Irvine, Materials Science and Engineering Palomba, Francesco; University of California Irvine, Biomedical Engineering Whiteson, Katrine; University of California Irvine, Molecular Biology and Biochemistry Digman, Michelle; University of California Irvine, Biomedical Engineering Siryaporn, Albert; University of California Irvine Hochbaum, Allon; University of California Irvine, Materials Science and Engineering

Rapid antibiotic susceptibility determination by fluorescence lifetime tracking of bacterial metabolism

Mauricio D. Rojas-Andrade[#,1], Kumar Perinbam[#,2], Quan Thanh Nguyen[2], Jonathan S. Kim[3], Francesco Palomba[4], Katrine Whiteson[3], Michelle A. Digman[4], Albert Siryaporn[2,3], Allon I. Hochbaum[*,1,3,5,6]

[1]Department of Materials Science and Engineering
University of California, Irvine,
Irvine, CA 92697 USA

[2]Department of Physics and Astronomy
University of California, Irvine
Irvine, CA 92697 USA

[3]Department of Molecular Biology and Biochemistry
University of California, Irvine
Irvine, CA 92697 USA

[4]Department of Biomedical Engineering
University of California, Irvine
Irvine, CA 92697 USA

[5]Department of Chemistry
University of California, Irvine,
Irvine, CA 92697 USA

[6]Department of Chemical and Biomolecular Engineering
University of California, Irvine,
Irvine, CA 92697 USA

[#]Authors contributed equally

*To whom correspondence should be addressed: hochbaum@uci.edu

Abstract

To combat the rise of antibiotic-resistance in bacteria and the resulting effects on healthcare worldwide, new technologies are needed that can perform rapid antibiotic susceptibility testing (AST). Conventional clinical methods for AST rely on growth-based assays which typically require long incubation times to obtain quantitative results, representing a major bottleneck in the determination of the optimal antibiotic regimen to treat patients. Here, we demonstrate a rapid AST method based on metabolic activity measured by fluorescence lifetime imaging microscopy (FLIM). Using lab strains and clinical isolates of *Escherichia coli* with tetracycline-susceptible and resistant phenotypes as models, we demonstrate that changes in metabolic state associated with antibiotic susceptibility can be quantitatively tracked by FLIM. Our results show that the magnitude of metabolic perturbation resulting from antibiotic activity correlates with susceptibility evaluated by conventional metrics. Moreover, susceptible and resistant phenotypes can be differentiated in as short as 10 minutes after antibiotic exposure. This FLIM-AST (FAST) method is applicable to other antibiotics and provides insights into the nature of metabolic perturbations inside bacterial cells resulting from antibiotic exposure with single cell resolution.

Keywords: Antibiotic Susceptibility Testing, Fluorescence Lifetime Imaging Microscopy, Phasor, Metabolism

The spread of antibiotic resistant bacteria poses a significant global public health concern. The rapid and accurate determination of susceptibility to antibiotics is one of the most effective strategies for mitigating this spread. Antibiotic susceptibility testing (AST) identifies the most effective antibiotic therapy and avoids the use of broad-spectrum antibiotics that contribute to the spread of antibiotic resistance. Current phenotypic assays relying on cell growth in liquid or solid media are the clinical standard for AST[1-4] but they require long time periods for microorganisms to demonstrate differentiable growth. In contrast, several genotypic assays such as PCR and genomic sequencing provide much more rapid detection of resistance genes through quantification of nucleotide biomarkers.[5-10] However, these technologies cannot detect uncharacterized resistance genes or phenotypic resistance, such as tolerance and persistence.[11]

The quantification of metabolic activity, on the other hand, shows promise for rapid, phenotypic AST.[12] Metabolomic analysis shows that exposure of susceptible bacteria to antibiotics induces significant changes in metabolite profiles within 30 minutes.[13] Fluorescence lifetime imaging microscopy (FLIM) is a label-free spectroscopic technique that rapidly and quantitatively assesses metabolic changes[14-15] at the single-cell level by measuring the ratio of free-to-enzyme bound metabolites and endogenous fluorophores, NAD(P)H.[16] The ratio of free-to-bound NAD(P)H in cellular environments is an accurate metric for metabolic activity of the cell as these cofactors are involved in several key metabolic pathways.[17-23] FLIM analysis of NAD(P)H fluorescence lifetimes can be represented in a two-dimensional phasor plot and provides a quantitative[16, 24] measurement of this ratio in eukaryotic[25] and prokaryotic[26] cells. Under metabolism-altering conditions, shifts in *g* and *s* components of NAD(P)H FLIM phasor are expected to directly correlate with changes in metabolic activity. Shifts towards smaller *g*-values indicate a lower free:bound NAD(P)H ratio, consistent with a model in

which metabolically active cells have a greater proportion of NAD(P)H-dependent enzymatic activity compared to more metabolically dormant cells. Indeed, FLIM identifies metabolic changes that occur in bacterial cells due to changes in nutrients,[26] virulence,[27] and antibiotic exposure.[17] The rapid analysis, metabolic quantitation, and the label-free nature of this method make it a highly attractive candidate for metabolic AST.

In this study, we utilize NAD(P)H FLIM analysis to rapidly assess metabolic changes of bacterial cells in response to antibiotic challenges. Using susceptible, resistant, and clinical isolates of *Escherichia coli* as model strains, we characterize dynamic changes in metabolic state during exposure to bacteriostatic (tetracycline, chloramphenicol) and bactericidal (gentamicin) antibiotics. By tracking shifts in FLIM signal as a function of time and antibiotic concentration, we successfully identified resistant and susceptible phenotypes in under an hour and validated these results with conventional growth-based assays. These results demonstrate that FLIM is a viable method for assessment of antibiotic susceptibility.

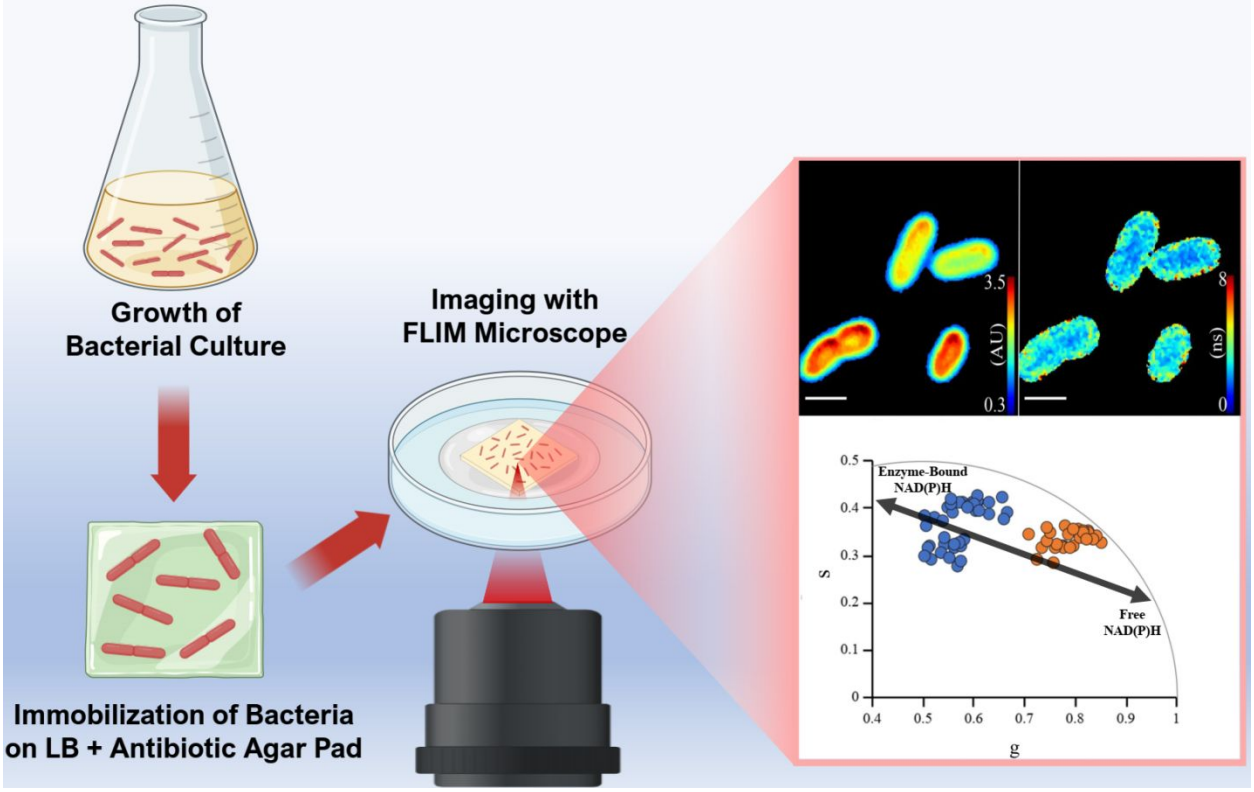

Figure 1. FLIM captures the dynamics of metabolic activity with single-cell resolution in immobilized bacterial cultures. Data insets show representative micrographs of fluorescence intensity (top left) and fluorescence lifetime (top right) across all pixels. Scale bars are 2 μm. Phasor representation of fluorescence lifetimes (bottom) is labeled with universal line (gray, solid), and eukaryotic (Black, arrows) NAD(P)H trajectory lines. AU is an arbitrary unit, ns is nanosecond.

Fluorescence lifetime imaging microscopy (FLIM) was used to quantitatively measure the effects of antibiotic action on bacterial metabolic activity and determine antibiotic susceptibility. Our methodology utilizes phasor analysis of fluorescence decay, which applies a

Fourier transform to fluorescence decay profiles generating real (*s*) and imaginary (*g*) components (see Supporting Information) which are then plotted as axes onto which fluorescence lifetimes are projected.[16, 24] Free and enzyme-bound NAD(P)H populate different regions of the phasor plot, with free NAD(P)H having a short fluorescence lifetime (~0.4 ns), being found at more positive *g*-values on the phasor plot, whereas bound NAD(P)H with longer (3-9 ns) lifetimes is located at smaller *g*-values.[25, 27-28] Experimentally acquired lifetimes typically lie between these two extrema and provide a measure of the ratio of free and enzyme-bound NAD(P)H for each pixel of the image (Figure 1). Under environmental perturbations such as antibiotic exposure, a shift in *g*-coordinate is indicative of the perturbation's effect on bacterial metabolic state (Figure 2A). Exposure of *E. coli* cells to bacteriostatic tetracycline for 1 h caused a shift to higher *g*-values. The magnitude of this shift provides a metric that quantifies the metabolic state change in response to antibiotic exposure. We first compared *g*-values of a tetracycline-susceptible wild-type *E. coli* strain (MG1655) with one harboring a tetracycline-resistance plasmid after exposure to 150 μg/mL tetracycline. Compared to antibiotic-free conditions, susceptible cells experienced a marked shift to more positive *g*-values after 1 h exposure whereas *g*-values of resistant cells only observed a slight increase under similar conditions (Figure 2B). Stark differences were also observed when challenging cells with 100 and 1000 μg/mL tetracycline (Figure 2C, S1), resulting in *g* shifts (Δ*g*) of +0.21 and +0.17 respectively for MG1655 cells, whereas resistant cells experienced insignificant shifts after an hour of exposure, even at 1000 μg/mL. At 1 and 10 μg/mL tetracycline, Δ*g* values were <0.05 for both types of cells. Notably, Δ*g* was slightly (~0.05) negative under control conditions, indicative of an increase in metabolic activity over an hour of exposure to antibiotic-free grown medium. These results are consistent with a model of tetracycline as a metabolism-suppressing bacteriostatic antibiotic.

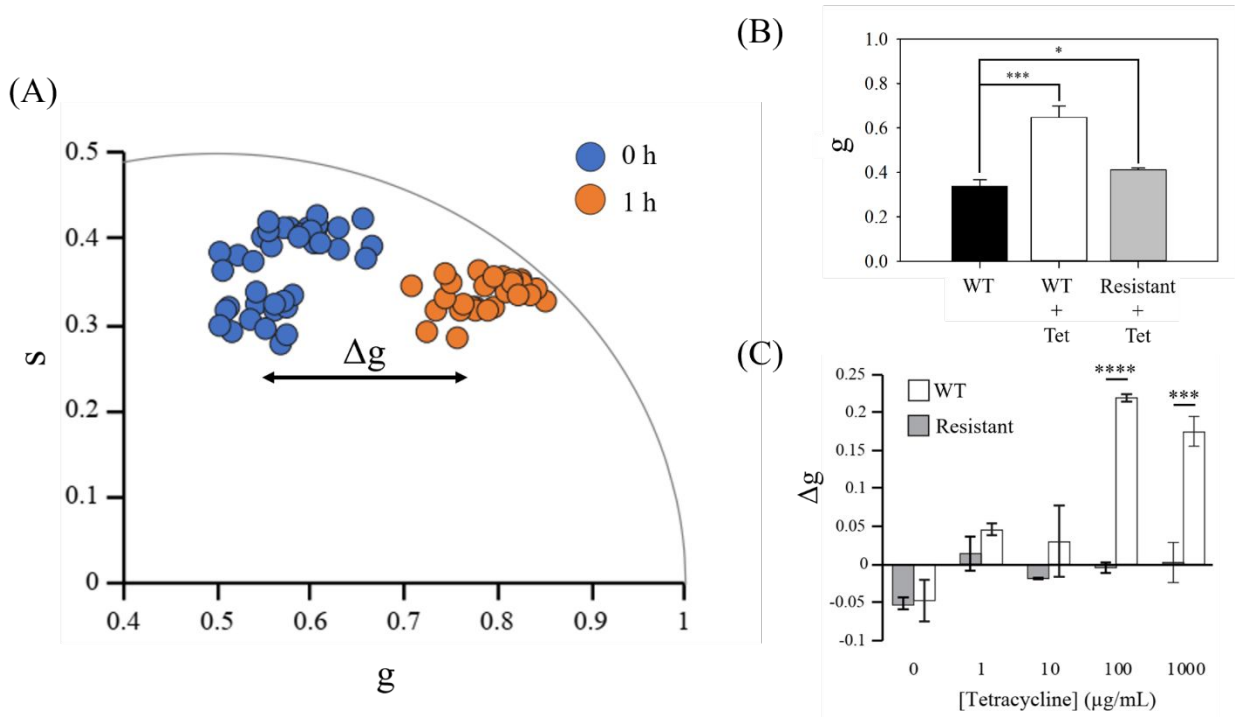

Figure 2. FLIM detects metabolic changes resulting from tetracycline exposure in *E. coli*. (A) FLIM phasor plot of *E. coli* MG1655 cells incubated on 1000 μg/mL tetracycline agar pads for 0 (blue) and 1 h (orange). Each point represents the average phasor position of a single cell within the population. (B) Comparison of average *g*-values for *E. coli* MG1655 and tetracycline-resistant cells after 1 h exposure

150 μg/mL tetracycline**.** (C) Change in average *g*-values after 1 h at various concentrations of tetracycline for *E. coli* MG1655 and resistant cells.

FLIM analysis of clinical *E. coli* isolates exposed to tetracycline was carried out to evaluate the potential of this technique for clinical application (*See Table S1 and Methods*). Δ*g* values of cells exposed to varying concentrations of tetracycline for 1 h show the same trend of increasing positive *g* value shifts with increasing tetracycline concentration for all strains (Figure 3A and S2). Large positive Δ*g* values were measured for most strains at 100 μg/mL tetracycline. *E. coli* 100 cells, however, exhibited a 2-fold lower Δ*g* compared to the other *E. coli* strains at this antibiotic concentration. The growth of *E. coli* 100 was correspondingly greater than the other strains when exposed to tetracycline (Figure 3B). At 1000 μg/mL tetracycline, similar large positive shifts were observed for all strains with values that are statistically similar. These data show that NAD(P)H FLIM correlates with tetracycline sensitivity of these strains and that the technique can identify strains with greater resistance to this antibiotic.

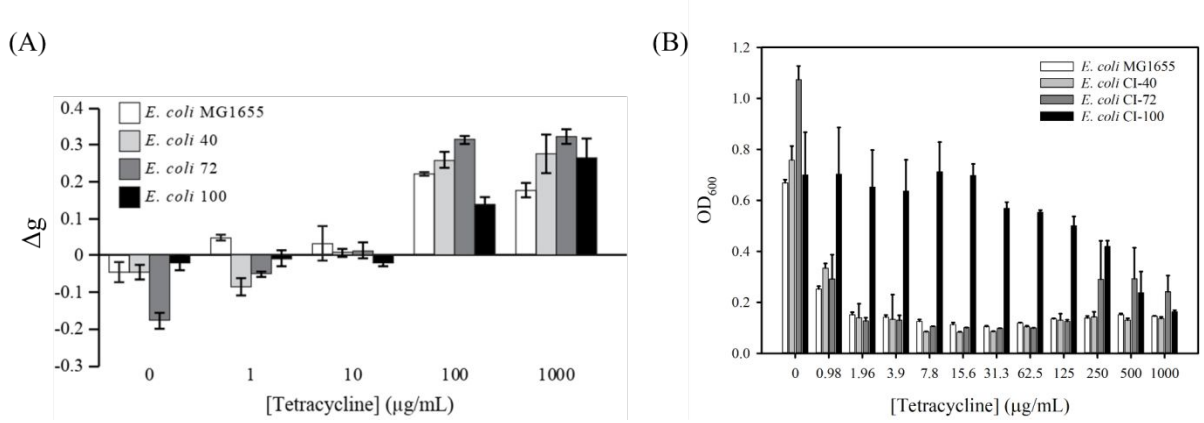

Figure 3. Tetracycline susceptibility of clinical isolates can be differentiated by FLIM analysis. (A) Comparison of changes in average *g* values for clinical *E. coli* isolates and *E. coli* MG1655 after 1 h growth on LB agar pads with varying concentrations of tetracycline. (B) Optical density (OD_{600}) of liquid *E. coli* cultures after 18 h growth in LB at varying tetracycline concentrations. Error bars in (B) correspond to standard deviation (N=5).

Antibiotics can be roughly classified as either bacteriostatic (growth suppressing) or bactericidal (killing) depending on their specific mechanism of action in the cell, and this distinction corresponds to differences in their effect on bacterial metabolism.[13,17,29,30] To investigate whether NAD(P)H FLIM can differentiate these metabolic effects, *E. coli* strains were challenged with gentamicin (bactericidal) and chloramphenicol (bacteriostatic). Growth inhibition assays show all these strains to be similarly susceptible to chloramphenicol (Figure S3), and clinical isolates *E. coli* 100 and *E. coli* 72 demonstrating greater resistance to gentamicin than the other strains (Figure S4). Exposure to chloramphenicol resulted in the expected positive shift in *g*-value corresponding to suppressed metabolic activity for all strains (Figure 4A). In contrast, negative shifts were observed in *E. coli* MG1655, 40 and 100 strains after gentamicin exposure (Figure 4B), consistent with toxic metabolic upregulation associated with bactericidal antibiotic activity.[13] *E. coli* 72, on the other hand, exhibited a smaller (~0.05) positive shift in *g*-value after exposure to gentamicin, despite having comparable sensitivity to gentamicin as *E. coli* 40. These results suggest that in *E. coli*, the metabolic effects of bacteriostatic antibiotics are characterized by a positive shift in *g* value whereas bactericidal antibiotic exposure in a negative shift at these concentrations and times of exposure. The deviation of the *E. coli* 72

isolate from the latter trend may be due to strain-specific differences in dynamics of the metabolic response to bactericidal antibiotics. Nevertheless, all *g*-value differences after 1 h exposure to chloramphenicol or gentamicin, positive or negative, are distinct from the null response of the tetracycline resistant strain, MG1655-pMG53, which shows no net change in response to tetracycline exposure at the same time point (Figure 2B,C).

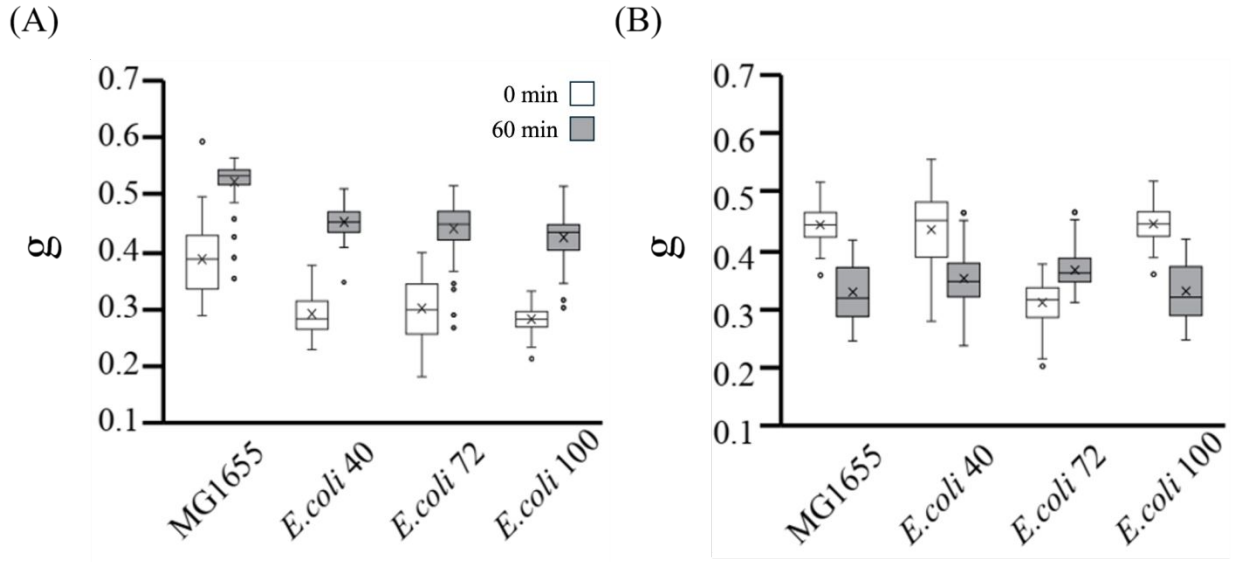

Figure 4. Different classes of antibiotics differentially affect the direction of *g*-value shift in the FLIM signal as a result of exposure. Average *g*-values for *E. coli* strains exposed to 1000 μg/mL (A) chloramphenicol and (B) gentamicin. Open and shaded boxes represent values measured at 0 and 60 min after exposure, respectively. The dots represent outlier data points. P << 0.0001 for comparisons of all 0 and 60 min *g* values of each strain and antibiotic exposure condition.

We expect that changes in *g*-value should depend on antibiotic exposure duration, since bacterial cells have time-dependent metabolic responses to antibiotic challenge.[13] In order to characterize temporal metabolic responses, time-course NAD(P)H FLIM measurements were taken of bacterial populations at 10 min intervals during exposure to antibiotics (Figure 5). A comparison of average *g*-values for *E. coli* MG1655 cells exposed to 100 μg/mL tetracycline or gentamicin shows a marked increase in *g*-value for tetracycline challenged cells, whereas gentamicin exposure caused a gradual decrease in *g*-value. In contrast, the average *g*-value changed very little (<10%) from the initial value without antibiotic exposure (Figure 5A) and for the resistant phenotype undergoing similar tetracycline exposure (Figure S5).

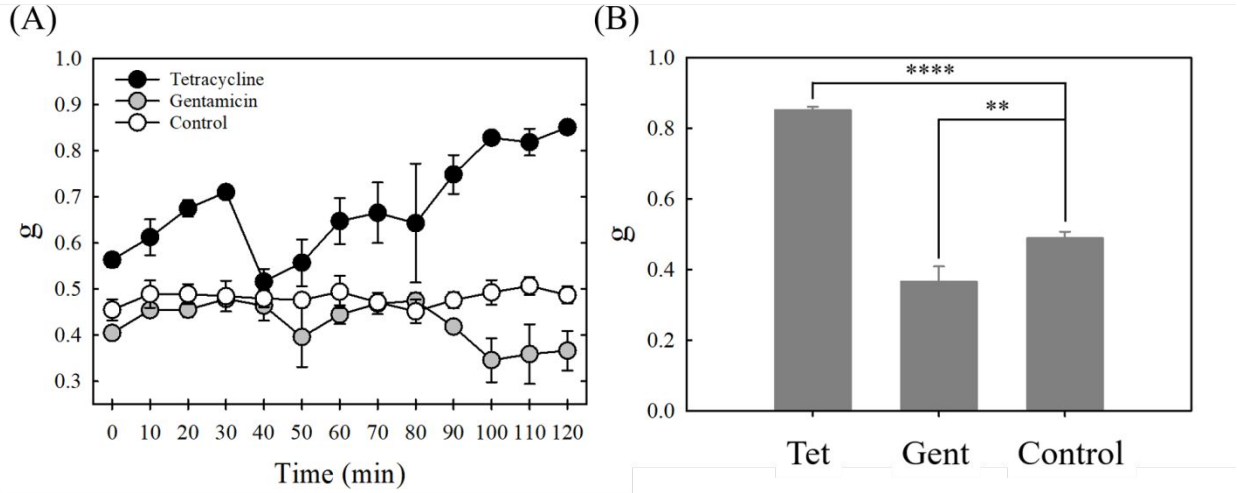

Figure 5. Temporal changes in *g*-value track with antibiotic mechanism. (A) Plot of average *g*-value over time for *E. coli* MG1655 cells during exposure to 150 µg/mL tetracycline, gentamicin, or without exposure (control). (B) Comparison of *g*-values after 2 h exposure to antibiotics.

To validate time-dependent changes in NAD(P)H FLIM signals, we utilized a conventional metabolic activity assay in planktonic *E. coli* cultures challenged by antibiotics. Resazurin (7-Hydroxy-3*H*-phenoxazin-3-one 10-oxide) is a membrane permeable cellular redox dye that yields a fluorescent product, resorufin, upon intracellular reduction and is widely used for assays of metabolic activity or bacterial viability.[31-33] Representative resorufin fluorescence profiles of *E. coli* MG1655 cultures grown in the presence of tetracycline (Figure 6A) and gentamicin (Figure 6B) show characteristic increases in resorufin fluorescence over time. Tetracycline exposure generally causes fluorescence to increase more slowly than the control without antibiotic. At 1000 µg/mL tetracycline, resorufin fluorescence increases more rapidly than at 1, 10, and 100 µg/mL exposure (Figure 6C), suggesting a greater metabolic activity than these concentrations until about 180 min. This observation agrees qualitatively with the NAD(P)H FLIM data (Figure 3A) suggesting less metabolic suppression at 1000 µg/mL than 100 µg/mL tetracycline, and perhaps indicating some bactericidal activity of tetracycline at especially high concentrations. In contrast to tetracycline, gentamicin causes resorufin fluorescence to increase more rapidly than the control culture conditions at early times (< 90 min) (Figure 6B,D), consistent with dysregulated metabolic effects of bactericidal antibiotic exposure. These trends are present in *E. coli* clinical isolates exposed to tetracycline (Figure S6B,D,F) and gentamicin (Figure S7B,D,F) and consistent with the trend in FLIM phasor *g* values of *E. coli* MG1655. The increased fluorescence of *E. coli* 100 at 1 and 10 µg/mL of tetracycline is consistent with a lack of metabolic suppression due to increased tetracycline resistance in this strain as compared to wild type. Corresponding growth and resorufin fluorescence profiles are shown for tetracycline and gentamicin exposure in Figure S6 and Figure S7 respectively. These results illustrate the metabolic perturbations that occur due to bacteriostatic or bactericidal antibiotics at the population level, and support the observations made at the single-cell level by NAD(P)H FLIM.

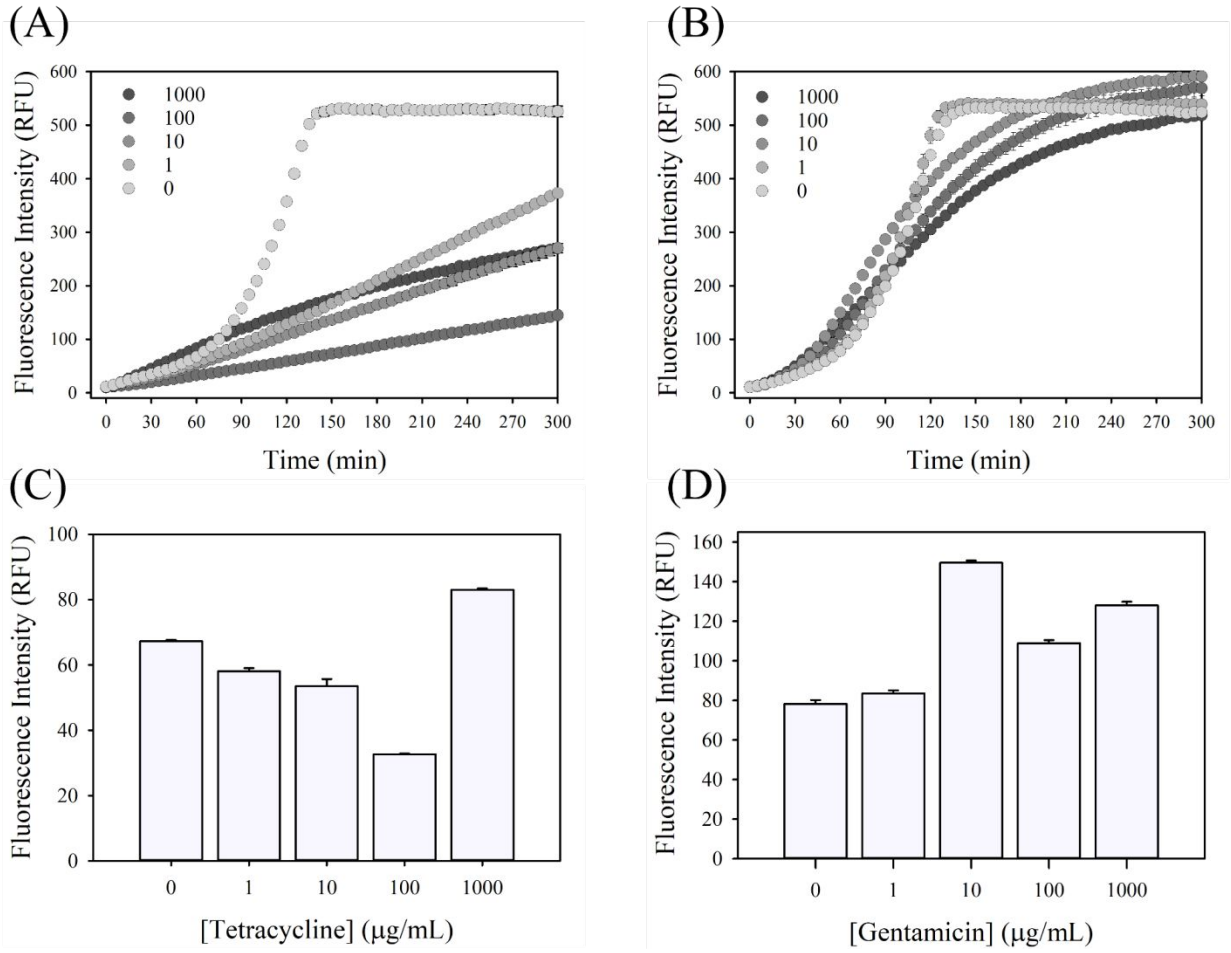

Figure 6. Resorufin fluorescence dynamics capture metabolic differences between bacteriostatic and bactericidal antibiotics. Resorufin fluorescence profiles of *E. coli* MG1655 cultures grown in LB at varying concentrations of (A) tetracycline and (B) gentamicin over time. Values in legends correspond to antibiotic concentrations in μg/mL. Comparison of average resorufin fluorescence values of *E. coli* MG1655 cultures after 60 min growth in (C) tetracycline and (D) gentamicin at the indicated concentrations.

Our results show that changes in the NAD(P)H FLIM phasor position of populations of bacteria are characteristic of susceptibility to antibiotics. FLIM *g*-values tracked with increasing concentration (Figure 2C, 3A) as well as duration (Figure 5A, S8) of antibiotic exposure, and were consistent with conventional metrics of growth inhibition (Figure 3B) and metabolic activity (Figure 6) in response to antibiotic exposure. Changes in *g*-values over the exposure period depend on both the antibiotic class and bacterial strain (Figure 4). The trends of *g*-values were different for bacteriostatic and bactericidal antibiotics, likely due to differences in the different impacts of these classes on metabolism[13, 34] (Fig 4, 5). The differences in *g*-value shifts between strains can be attributed to dependent variations in antibiotic susceptibility, consistent with conventional growth inhibition assay results (Figure 3, S3, S4). This approach discriminated between susceptible and non-susceptible strains in as little as 10 min (Figure 5A, S9). In contrast to existing standardized AST technologies such as disc-diffusion assays and broth microdilution, FLIM offers comparable differentiation of susceptible and resistant phenotypes at much shorter time scales.[35] In comparison to genotypic assays, FLIM-AST accounts for novel

resistance genes and non-genetically encoded resistance mechanisms, such as tolerance, which would otherwise give false negative outcomes in genotypic AST. These changes in FLIM signal are consistent across antibiotics within the same class and across most strains. Further benchmarking work is required to establish the robustness of this technique to the many species and patient-adapted characteristics of other pathogens and clinical isolates.

The interpretation of larger *g* values representing bacterial states with suppressed metabolic activity is consistent with lower resorufin fluorescence under similar conditions (Figure 6A). Resorufin fluorescence is conventionally used as a metric of cell viability[31] and metabolic activity, the change of which provides a metric of instantaneous metabolic trajectory in this study. A positive shift in *g*-value is also in agreement with tetracycline's mechanism of action, characterized by inhibition of aminoacyl-tRNA binding to bacterial ribosomal (30S, 70S) A sites, which results in decreased levels of enzymes involved in central metabolism (glycolysis/gluconeogenesis, TCA cycle, pyruvate metabolism).[36-37] Consistent with the effects of tetracycline, exposure of *E. coli* cells to chloramphenicol, another bacteriostatic antibiotic, also caused a shift to larger *g*-values (Figure 4A).

Bactericidal antibiotics, on the other hand, differ in their effect on bacterial metabolic pathways. They accelerate cellular respiration as a critical feature of their lethality.[13, 30, 34] Indeed, exposure to gentamicin was found to cause shifts towards smaller *g*-values (Figure 4B and Figure 5A), suggesting a decrease in free:bound NAD(P)H and, correspondingly, greater metabolic activity. This result can be rationalized given that gentamicin disrupts both translational accuracy and ribosome translocation.[38-39] This mistranslation results in accelerated metabolic activity[34] and toxic perturbations of the TCA cycle and central metabolism[13], in agreement with our observed shift in FLIM signal. The accelerating effect of gentamicin on metabolism was further substantiated by resorufin fluorescence assay (Figure 6D) which showed an increase in metabolic activity at early times for all gentamicin concentrations, in contrast to cultures exposed to low and moderate concentrations of tetracycline (Figure 6A), for which resorufin fluorescence was suppressed relative to the control. A longer exposure time (> 2 h) is required to observe significant differences in *g*-values for gentamicin-challenged cells as illustrated in Figure 5, likely due to the complex interplay of metabolic stimulation and cytotoxic effects.

Using shifts in FLIM phasor *g*-values in response to antibiotic exposure, susceptible and resistant phenotypes were easily differentiated at clinically relevant time scales. Tetracycline susceptible *E. coli* strains exhibited a marked shift to more positive *g*-values over the exposure period whereas the resistant *E. coli* MG1655-pMG53 strain (Figure 2C and S9) showed very little change under similar conditions. We observed that for bactericidal antibiotics, metabolic changes are complex and diverge from initial trajectories after extended periods of time (Figure 6B).[13, 30, 40] This is possibly the reason behind *E. coli* 72 showing a positive shift in *g*-value (Figure 4B) as metabolic perturbations could occur in different stages, or cause oscillations in metabolic trajectory. It is possible that the decrease in *g*-value observed for *E. coli* MG1655, 40*,* and 100*,* and increase in *g*-value for *E. coli* 72 are due to the sensitivity of the time point of measurement around 1 h which occurs before the abrupt decrease in *g*-value seen in the time-resolved gentamicin resorufin profile (Figure 5A). The divergence of short-term metabolic trajectories may be dependent on the specific antibiotic mechanism of action, suggesting initial benchmarking of other antibiotics as best practice before accurate susceptibility analysis can be carried out. Additionally, the specific resistance mechanism(s) utilized by bacteria to survive antibiotic exposure can also have convoluting effects on metabolic processes, further complicating static NAD(P)H FLIM measurements to assess susceptibility. Surmounting these

challenges will require further investigation into temporal changes in FLIM response at short timescales, especially for bactericidal antibiotic exposure.

Conclusion

We demonstrated a FLIM-based imaging method that can determine the antibiotic susceptibility of bacteria by quantifying metabolic changes in response to antibiotic challenge. This method significantly improves upon conventional AST methodology by reducing the time required to differentiate resistant and susceptible strains to as little as 10 min, with even better resolved differentiation after 1-2 h. Additionally, we have shown this method's clinical applicability by accurately determining differential antibiotic susceptibility for clinical *E. coli* isolates in addition to resistant and susceptible laboratory *E. coli* strains. While the present FLIM analysis and measurement setup is not appropriate for direct application in clinical settings, but miniaturized FLIM systems have been developed and further work to streamline sample preparation, data collection, and automated analysis will bring this technology closer to a viable AST product. This work not only provides a platform for next-generation metabolic AST technology, but also represents a promising screening method for antibiotic classification based on metabolic perturbations.

Methods

Strains and growth conditions

Bacteria used in this study include lab and clinical strains (Table S1); *E. coli* isolated from infants with Urinary Tract Infections at the Children's Hospital Orange County were collected with approval from IRB#120775. Strains were streaked onto luria broth (LB) agar plates from 20% (v/v) glycerol frozen stocks. Liquid cultures were first grown overnight (~16 h) from single colonies in 3 mL LB, diluted to 0.1 OD_{600} in fresh LB, and then sub-cultured in 3 mL aliquots for 5 h. For FLIM analysis, a 2 µL drop of the resulting cell suspension was pipetted onto a microscope dish (Ibidi) and an LB agar pad (1 cm x 1 cm x 0.25 cm) placed on top of it to immobilize bacterial cells. Antibiotic exposure was achieved by diluting concentrated antibiotic (tetracycline, gentamicin, chloramphenicol) solutions to the desired concentration in the LB agar solution prior to pouring and cutting. The microscope dish was immediately placed in an environmentally controlled microscope stage at 37 C and bacteria were imaged immediately to obtain profiles at 0 min and every 10 min for temporal tracking experiments or after 60 min for static measurements.

Fluorescence lifetime imaging microscopy

Micrographs were acquired using a custom-built multiphoton microscope utilizing an Olympus FV1000 system and an Olympus IX81 microscope (Olympus, Waltham, Massachusetts) as described previously.[23] For multiphoton excitation, the microscope employs an 80 MHz ultrafast Ti:Sapphire Mai Tai laser (Spectra-Physics, Santa Clara, CA) set at 740 nm. A PlanApo N Olympus oil-immersion 60x (1.42 NA) objective (Olympus, Waltham, MA) was used to find and image regions of interest (ROIs). Emission light was separated using a 690-nm SP dichroic 460/80-nm filter pair. An H7422P-40 photomultiplier tube module (Hamamatsu, Bridgewater, NJ) and A320 FastFLIM Box (ISS, Champaign, IL) were used to measure

fluorescence lifetime. The microscope was calibrated before each session by setting the fluorescence lifetime obtained for 4 μM coumarin 6G (Sigma) in ethanol to 2.5 ns. The laser power was set at 20% (< 3 mW at the back aperture of the microscope) using an acousto-optic modulator (AA Opto Electronic, Orsay, France). Fluorescence lifetimes were collected using the 10x or 25x digital zoom mode at a rate of 1.7 s/frame. Image acquisition was controlled by SimFCS software version 4 (64-bit) (Laboratory for Fluorescence Dynamics, Irvine, CA). The pixel dwell time for data acquired from all samples was 20 *μ*s/pixel. The average number of photons per pixel per frame scan across the entire region of interest varies from about 2-36 (Figure S10). For all measurements, 50 sequential frames were acquired from each ROI to generate a single FLIM image. Masks for lifetime data from bacterial cells were created through SimFCS using fluorescence intensity images and image intensity thresholding. See reference 27 for a more detailed workflow. The signal to noise ratio for all conditions range between about 1.5-10 across all conditions (Figure S11). Cells are distinguished from the surrounding agar background signal by both fluorescence intensity and lifetime (Figures S12-14). The number of cells analyzed in each condition are detailed in Table S2. For time lapse data, images were acquired in the same way as described above from a single ROI at 10 minute intervals. We do not see the evolution of long lifetime species expected with photobleaching processes and the fluorescence intensity of cells in the same ROI over time do not show evidence of photodegradation (Figure S15).

FLIM data used in this study is publicly available at https://idr.openmicroscopy.org/.

Growth Inhibition Assays

Liquid cultures were first prepared as described above. A 2-fold serial dilution of each antibiotic was prepared in a range from 1000 μg/mL to 0.97 μg/mL. Antibiotic stock solutions were initially prepared at 10x concentrations starting at 10,000 μg/mL using ultrapure deionized (DI) water (Barnstead E-Pure) as the solvent, adjusting for antibiotic purity according to the certificate of analysis (CoA). A serial dilution of ten 2-fold dilutions were prepared by adding 0.5 mL of the 10,000 μg/mL solution to 0.5 mL of DI water and vortexing to mix. Fresh antibiotic solutions were prepared daily for each experiment and 20 μL of 10x solutions were added to the wells of 96-well plates (Costar™). After the 5 h sub-culture, cell suspensions were diluted to 0.1 OD_{600} in fresh LB and 180 μL of the re-diluted cell suspension was added to wells of the 96-well plates to dilute the antibiotics to the final concentrations (1000 μg/mL to 0.97 μg/mL). Each plate was inoculated with a single bacterial strain and tested against one antibiotic, with five technical replicates per antibiotic concentration. Antibiotic-challenged bacterial cultures were subsequently grown at 37 C in a shaking incubation chamber. Optical density at 600 nm (OD_{600}) was measured using a Varioskan LUX microplate reader (Thermo Fisher Scientific) every 15 minutes over 18 h of growth. For tetracycline plates, we observed accumulation of cells at the bottom of wells of clinical isolate cultures at high tetracycline concentrations, causing an unexpected increase in OD_{600} readings at these concentrations (Figure S16). Consequently, readings of tetracycline growth inhibition were taken from 100 μL aliquots of only planktonic cells from these well plates transferred to a clean plate. Care was taken not to disturb the sediment when pipetting to the clean plate, and OD_{600} values were pathlength corrected to be comparable to the other antibiotic plates. Spot titer cell viability assays validate the OD_{600} readings taken in this way (Figure S17)

Tracking aggregate metabolic activity of bacterial cultures by resazurin reduction

Preparation of liquid cultures followed the same protocol described in the growth inhibition assays. To each well, 140 µL of the re-diluted cell suspension followed by 20 µL antibiotic solutions (10, 1, 0.1, 0.01 mg/mL) to a final antibiotic concentration of 1000, 100, 10, and 1 ug/mL, and 40 µL of a 125 µg/mL resazurin solution (PBS, pH=7.4) was added bringing the final volume to 200 µL. Antibiotic-challenged bacterial cultures were subsequently grown at 37 C in a Varioskan LUX microplate reader with optical density at 700 nm (OD_{700}) and fluorescence intensity at 585 nm after excitation at 490 nm read every 5 min with continuous shaking between reads.

Statistical Analysis

Data for Box-Whisker plots are expressed as minimum, first quartile, median, third quartile, and maximum, with outliers indicated by dots and all other data expressed as the mean ± standard deviation. Statistical significance of differences in mean values of FLIM phasor coordinates were evaluated by two-tailed heteroscedastic (un-paired) t-test because different ROIs, and therefore different numbers of cells (Table S2), were used to collect data at 0 and 60 or 120 min of exposure to antibiotics. Where indicated, **** = $P < 0.0001$, *** = $P < 0.001$, ** = $P < 0.01$, and * = $P < 0.05$. Values $P < 0.05$ were considered statistically significant.

Author Contributions

MDR, KP, KW, AS, and AIH conceived of the project and designed experiments. All authors collectively discussed the results. MDR, KP, JSK and QAN conducted experiments and analyzed data. FP helped analyzed FLIM data to address reviewer comments. KW provided the *E. coli* clinical isolates used in this study. MAD provided access to the FLIM microscope and consulted on data interpretation.

Acknowledgements

AIH and MDRA acknowledge support from NSF CHE-1808332. KP and AS acknowledge support from NIH NIAID R21AI139968. All authors acknowledge support from UCI Beall Applied Innovation Proof of Product award. The experiments reported in this paper were performed at the Laboratory for Fluorescence Dynamics (LFD) at the University of California, Irvine, which is supported jointly by the National Institutes of Health (2P41GM103540) and UC Irvine. Figure 1 was created with BioRender.com. We would like to thank Dr. Antonia Arrieta and Stephanie Osborne from the Children's Hospital of Orange County for sharing *E. coli* isolates from a study of infants with urinary tract infections (IRB#120775).

References

1. Jenkins, S. G.; Schuetz, A. N., Current concepts in laboratory testing to guide antimicrobial therapy. *Mayo Clin Proc* **2012,** *87* (3), 290-308.
2. Khan, Z. A.; Siddiqui, M. F.; Park, S., Current and Emerging Methods of Antibiotic Susceptibility Testing. *Diagnostics (Basel)* **2019,** *9* (2).
3. Jorgensen, J. H.; Ferraro, M. J., Antimicrobial susceptibility testing: a review of general principles and contemporary practices. *Clin Infect Dis* **2009,** *49* (11), 1749-55.

4. Matuschek, E.; Brown, D. F.; Kahlmeter, G., Development of the EUCAST disk diffusion antimicrobial susceptibility testing method and its implementation in routine microbiology laboratories. *Clin Microbiol Infect* **2014,** *20* (4), O255-66.
5. Martineau, F.; Picard, F. J.; Grenier, L.; Roy, P. H.; Ouellette, M.; Bergeron, M. G., Multiplex PCR assays for the detection of clinically relevant antibiotic resistance genes in staphylococci isolated from patients infected after cardiac surgery. The ESPRIT Trial. *J Antimicrob Chemother* **2000,** *46* (4), 527-34.
6. Rossney, A. S.; Herra, C. M.; Brennan, G. I.; Morgan, P. M.; O'Connell, B., Evaluation of the Xpert methicillin-resistant Staphylococcus aureus (MRSA) assay using the GeneXpert real-time PCR platform for rapid detection of MRSA from screening specimens. *J Clin Microbiol* **2008,** *46* (10), 3285-90.
7. Wong, L. K.; Hemarajata, P.; Soge, O. O.; Humphries, R. M.; Klausner, J. D., Real-Time PCR Targeting the penA Mosaic XXXIV Type for Prediction of Extended-Spectrum-Cephalosporin Susceptibility in Clinical Neisseria gonorrhoeae Isolates. *Antimicrob Agents Chemother* **2017,** *61* (11).
8. Abram, T. J.; Cherukury, H.; Ou, C. Y.; Vu, T.; Toledano, M.; Li, Y. Y.; Grunwald, J. T.; Toosky, M. N.; Tifrea, D. F.; Slepenkin, A.; Chong, J.; Kong, L. S.; Del Pozo, D. V.; La, K. T.; Labanieh, L.; Zimak, J.; Shen, B.; Huang, S. S.; Gratton, E.; Peterson, E. M.; Zhao, W. A., Rapid bacterial detection and antibiotic susceptibility testing in whole blood using one-step, high throughput blood digital PCR. *Lab Chip* **2020,** *20* (3), 477-489.
9. Koser, C. U.; Bryant, J. M.; Becq, J.; Torok, M. E.; Ellington, M. J.; Marti-Renom, M. A.; Carmichael, A. J.; Parkhill, J.; Smith, G. P.; Peacock, S. J., Whole-genome sequencing for rapid susceptibility testing of M. tuberculosis. *N Engl J Med* **2013,** *369* (3), 290-2.
10. Colman, R. E.; Anderson, J.; Lemmer, D.; Lehmkuhl, E.; Georghiou, S. B.; Heaton, H.; Wiggins, K.; Gillece, J. D.; Schupp, J. M.; Catanzaro, D. G.; Crudu, V.; Cohen, T.; Rodwell, T. C.; Engelthaler, D. M., Rapid Drug Susceptibility Testing of Drug-Resistant Mycobacterium tuberculosis Isolates Directly from Clinical Samples by Use of Amplicon Sequencing: a Proof-of-Concept Study. *J Clin Microbiol* **2016,** *54* (8), 2058-67.
11. Balaban, N. Q.; Helaine, S.; Lewis, K.; Ackermann, M.; Aldridge, B.; Andersson, D. I.; Brynildsen, M. P.; Bumann, D.; Camilli, A.; Collins, J. J.; Dehio, C.; Fortune, S.; Ghigo, J. M.; Hardt, W. D.; Harms, A.; Heinemann, M.; Hung, D. T.; Jenal, U.; Levin, B. R.; Michiels, J.; Storz, G.; Tan, M. W.; Tenson, T.; Van Melderen, L.; Zinkernagel, A., Definitions and guidelines for research on antibiotic persistence. *Nat Rev Microbiol* **2019,** *17* (7), 441-448.
12. Yang, K.; Li, H. Z.; Zhu, X.; Su, J. Q.; Ren, B.; Zhu, Y. G.; Cui, L., Rapid Antibiotic Susceptibility Testing of Pathogenic Bacteria Using Heavy-Water-Labeled Single-Cell Raman Spectroscopy in Clinical Samples. *Anal Chem* **2019,** *91* (9), 6296-6303.
13. Belenky, P.; Ye, J. D.; Porter, C. B. M.; Cohen, N. R.; Lobritz, M. A.; Ferrante, T.; Jain, S.; Korry, B. J.; Schwarz, E. G.; Walker, G. C.; Collins, J. J., Bactericidal Antibiotics Induce Toxic Metabolic Perturbations that Lead to Cellular Damage. *Cell Rep* **2015,** *13* (5), 968-980.
14. Lee, D. H.; Li, X.; Ma, N.; Digman, M. A.; Lee, A. P., Rapid and label-free identification of single leukemia cells from blood in a high-density microfluidic trapping array by fluorescence lifetime imaging microscopy. *Lab Chip* **2018,** *18* (9), 1349-1358.
15. Ma, N.; Kamalakshakurup, G.; Aghaamoo, M.; Lee, A. P.; Digman, M. A., Label-Free Metabolic Classification of Single Cells in Droplets Using the Phasor Approach to Fluorescence Lifetime Imaging Microscopy. *Cytom Part A* **2019,** *95a* (1), 93-100.
16. Digman, M. A.; Caiolfa, V. R.; Zamai, M.; Gratton, E., The phasor approach to fluorescence lifetime imaging analysis. *Biophysical Journal* **2008,** *94* (2), L14-L16.
17. Bhattacharjee, A.; Datta, R.; Gratton, E.; Hochbaum, A. I., Metabolic fingerprinting of bacteria by fluorescence lifetime imaging microscopy. *Sci Rep-Uk* **2017,** *7*.

18. Vishwasrao, H. D.; Heikal, A. A.; Kasischke, K. A.; Webb, W. W., Conformational dependence of intracellular NADH on metabolic state revealed by associated fluorescence anisotropy. *Journal of Biological Chemistry* **2005,** *280* (26), 25119-25126.
19. Heikal, A. A., Intracellular coenzymes as natural biomarkers for metabolic activities and mitochondrial anomalies. *Biomark Med* **2010,** *4* (2), 241-263.
20. Drozdowicz-Tomsia, K.; Anwer, A. G.; Cahill, M. A.; Madlum, K. N.; Maki, A. M.; Baker, M. S.; Goldys, E. M., Multiphoton fluorescence lifetime imaging microscopy reveals free-to-bound NADH ratio changes associated with metabolic inhibition. *J Biomed Opt* **2014,** *19* (8).
21. Chakraborty, S.; Nian, F. S.; Tsai, J. W.; Karmenyan, A.; Chiou, A., Quantification of the Metabolic State in Cell-Model of Parkinson's Disease by Fluorescence Lifetime Imaging Microscopy. *Sci Rep-Uk* **2016,** *6*.
22. Evers, M.; Salma, N.; Osseiran, S.; Casper, M.; Birngruber, R.; Evans, C. L.; Manstein, D., Enhanced quantification of metabolic activity for individual adipocytes by label-free FLIM. *Sci Rep-Uk* **2018,** *8*.
23. Kalinina, S.; Freymueller, C.; Naskar, N.; von Einem, B.; Reess, K.; Sroka, R.; Rueck, A., Bioenergetic Alterations of Metabolic Redox Coenzymes as NADH, FAD and FMN by Means of Fluorescence Lifetime Imaging Techniques. *Int J Mol Sci* **2021,** *22* (11).
24. Ma, N.; Digman, M. A.; Malacrida, L.; Gratton, E., Measurements of absolute concentrations of NADH in cells using the phasor FLIM method. *Biomed Opt Express* **2016,** *7* (7), 2441-2452.
25. Wright, B. K.; Andrews, L. M.; Markham, J.; Jones, M. R.; Stringari, C.; Digman, M. A.; Gratton, E., NADH distribution in live progenitor stem cells by phasor-fluorescence lifetime image microscopy. *Biophys J* **2012,** *103* (1), L7-9.
26. Torno, K.; Wright, B. K.; Jones, M. R.; Digman, M. A.; Gratton, E.; Phillips, M., Real-time Analysis of Metabolic Activity Within Lactobacillus acidophilus by Phasor Fluorescence Lifetime Imaging Microscopy of NADH. *Curr Microbiol* **2013,** *66* (4), 365-367.
27. Perinbam, K.; Chacko, J. V.; Kannan, A.; Digman, M. A.; Siryaporn, A., A Shift in Central Metabolism Accompanies Virulence Activation in Pseudomonas aeruginosa. *mBio* **2020,** *11* (2).
28. Skala, M. C.; Riching, K. M.; Gendron-Fitzpatrick, A.; Eickhoff, J.; Eliceiri, K. W.; White, J. G.; Ramanujam, N., In vivo multiphoton microscopy of NADH and FAD redox states, fluorescence lifetimes, and cellular morphology in precancerous epithelia. *Proc Natl Acad Sci U S A* **2007,** *104* (49), 19494-9.
29. Kohanski, M. A.; Dwyer, D. J.; Collins, J. J., How antibiotics kill bacteria: from targets to networks. *Nat Rev Microbiol* **2010,** *8* (6), 423-435.
30. Dwyer, D. J.; Belenky, P. A.; Yang, J. H.; MacDonald, I. C.; Martell, J. D.; Takahashi, N.; Chan, C. T. Y.; Lobritz, M. A.; Braff, D.; Schwarz, E. G.; Ye, J. D.; Pati, M.; Vercruysse, M.; Ralifo, P. S.; Allison, K. R.; Khalil, A. S.; Ting, A. Y.; Walker, G. C.; Collins, J. J., Antibiotics induce redox-related physiological alterations as part of their lethality. *P Natl Acad Sci USA* **2014,** *111* (20), E2100-E2109.
31. Ishiyama, M.; Furusawa, H.; Shiga, M.; Ohseto, F.; Sasamoto, K., A resorufin derivative as a fluorogenic indicator for cell viability. *Anal Sci* **1999,** *15* (10), 1025-1028.
32. Gonzalez-Pinzon, R.; Haggerty, R.; Myrold, D. D., Measuring aerobic respiration in stream ecosystems using the resazurin-resorufin system. *J Geophys Res-Biogeo* **2012,** *117*.
33. Mehring, A.; Erdmann, N.; Walther, J.; Stiefelmaier, J.; Strieth, D.; Ulber, R., A simple and low-cost resazurin assay for vitality assessment across species. *J Biotechnol* **2021,** *333*, 63-66.
34. Lobritz, M. A.; Belenky, P.; Porter, C. B. M.; Gutierrez, A.; Yang, J. H.; Schwarz, E. G.; Dwyer, D. J.; Khalil, A. S.; Collins, J. J., Antibiotic efficacy is linked to bacterial cellular respiration. *P Natl Acad Sci USA* **2015,** *112* (27), 8173-8180.
35. Syal, K.; Mo, M.; Yu, H.; Iriya, R.; Jing, W.; Guodong, S.; Wang, S.; Grys, T. E.; Haydel, S. E.; Tao, N., Current and emerging techniques for antibiotic susceptibility tests. *Theranostics* **2017,** *7* (7), 1795-1805.

36. Gale, E. F., *The Molecular basis of antibiotic action*. Wiley: London, New York,, 1972; p xviii, 456 p.
37. Lin, X. M.; Kang, L. Q.; Li, H.; Peng, X. X., Fluctuation of multiple metabolic pathways is required for Escherichia coli in response to chlortetracycline stress. *Molecular Biosystems* **2014,** *10* (4), 901-908.
38. Yoshizawa, S.; Fourmy, D.; Puglisi, J. D., Structural origins of gentamicin antibiotic action. *Embo J* **1998,** *17* (22), 6437-6448.
39. Zhang, J. J.; Pavlov, M. Y.; Ehrenberg, M., Accuracy of genetic code translation and its orthogonal corruption by aminoglycosides and Mg2+ ions. *Nucleic Acids Research* **2018,** *46* (3), 1362-1374.
40. Kohanski, M. A.; Dwyer, D. J.; Hayete, B.; Lawrence, C. A.; Collins, J. J., A common mechanism of cellular death induced by bactericidal antibiotics. *Cell* **2007,** *130* (5), 797-810.

For Table of Contents Use Only

Rapid antibiotic susceptibility determination by fluorescence lifetime tracking of bacterial metabolism

Mauricio D. Rojas-Andrade[#,1], Kumar Perinbam[#,2], Quan Thanh Nguyen[2], Jonathan S. Kim[3], Francesco Palomba[4], Katrine Whiteson[3], Michelle A. Digman[4], Albert Siryaporn[2,3], Allon I. Hochbaum[*,1,3,5,6]